2015

A real-time plant discrimination system utilising discrete reflectance spectroscopy

Paul Symonds
Edith Cowan University

Arie Paap
Edith Cowan University

Kamal Alameh
Edith Cowan University

J Rowe

C Miller

10.1016/j.compag.2015.07.011
Symonds, P., Paap, A., Alameh, K., Rowe, J., & Miller, C. (2015). A real-time plant discrimination system utilising discrete reflectance spectroscopy. *Computers and Electronics in Agriculture*, *117*, 57-69. Available here

Computers and Electronics in Agriculture 117 (2015) 57–69

Contents lists available at ScienceDirect

Computers and Electronics in Agriculture

journal homepage: www.elsevier.com/locate/compag

Original papers

A real-time plant discrimination system utilising discrete reflectance spectroscopy

P. Symonds [a,*], A. Paap [a], K. Alameh [a], J. Rowe [b], C. Miller [b]

[a] Electron Science Research Institute, Edith Cowan University, Joondalup, WA 6027, Australia
[b] Photonic Detection Systems Pty. Ltd., Subiaco, WA 6008, Australia

ARTICLE INFO

Article history:
Received 17 July 2014
Received in revised form 21 February 2015
Accepted 21 July 2015
Available online 3 August 2015

Keywords:
Precision agriculture
Spectral reflectance
Optoelectronics
Embedded systems
Sensing
Real-time weed discrimination

ABSTRACT

An advanced, proof-of-concept real-time plant discrimination system is presented that employs two visible (red) laser diodes (635 nm, 685 nm) and one near-infrared (NIR) laser diode (785 nm). The lasers sequentially illuminate the target ground area and a linear sensor array measures the intensities of the reflected laser beams. The spectral reflectance measurements are then processed by an embedded microcontroller running a discrimination algorithm based on dual Normalised Difference Vegetation Indices (NDVI). Pre-determined plant spectral signatures are used to define unique regions-of-classification for use by the discrimination algorithm. Measured aggregated NDVI values that fall within a region-of-classification (RoC) representing an unwanted plant generate a spray control signal that activates an external spray module, thus allowing for a targeted spraying operation. Dynamic outdoor evaluation of the advanced, proof-of-concept real-time plant discrimination system, using three different plant species and control data determined under static laboratory conditions, shows that the system can perform green-from-green plant detection and accomplish practical discrimination for a vehicle speed of 3 km/h.

1. Introduction

To maximise crop yield, blanket spraying of herbicides and insecticides is commonly used for weed and pest management. The application of such chemicals is often done terrestrially using an appropriately configured tractor or aerially, using a crop duster. A cost effective system for weed control, using spot-spraying of herbicides at appropriate periods during the cultivation cycle, is of interest to farmers due to the associated benefits of managed costs, reduced herbicide application and crop yield optimisation.

In recent years, the collective application of new technological advancements and improved management practices to farming has given rise to the field of Precision Agriculture (PA) (Zhang et al., 2002), of which a major aspect is Site-Specific Crop Management (SSCM) for optimised, efficient field-crop production. The management of weeds through an agricultural crop's growth cycle, is one such area that has attracted considerable research interest. Reviews by Zwiggelaar (1998) and Noble et al. (2002) have concluded that weed/soil (green-from-brown) and crop/weed (green-from-green) discrimination, utilising spectral reflectance and hyperspectral/multispectral imaging techniques, has achieved varying levels of success. In particular, spectral analysis has been used as a method for discriminating plants from soil (green-from-brown discrimination) (Felton and McCloy, 1992; Brownhill, 2006). Fundamental work presented by Wang et al. (2001) quantifies plant spectral characteristics by using five feature wavelengths and four normalised colour indices for crop/weed (green-from-green) discrimination. The work led to the development of an optical weed sensor capable of detecting wheat from specific weeds under controlled laboratory conditions. More recently, Deng et al. (2014) have investigated the application of Support Vector Machine (SVM), Artificial Neural Network (ANN) and Decision Tree (DT) based classifiers to compare the classification rates for plant spectral measurements taken in the 350–760 nm visible wavelength range and the 350–2500 nm visible and NIR wavelength range. Experimentally, spectral irradiance measurements for the test crop (corn) and weeds (*Dchinochloa crasgalli* and *Echinochloa crusgalli*) were performed in the field, using a handheld spectroradiometer, with results showing that the visible light range proved adequate to meet discrimination requirements for the given test plants. An innovative approach presented by Sahba et al. (2006) and Paap et al. (2008) demonstrated generalised green-from-green discrimination using a novel optical architecture, with the eventual objective of practical application of the technology to weed treatment, using spot spraying in

* Corresponding author. Tel.: +61 08 6304 2366; fax: +61 08 6304 2908.
E-mail address: p.symonds@ecu.edu.au (P. Symonds).

http://dx.doi.org/10.1016/j.compag.2015.07.011
0168-1699/

field-crop production. The application of hyperspectral measurement techniques to the problem of crop/weed discrimination has also been reported on in the literature. Shapira et al. (2010) have investigated using ground based hyperspectral imaging to detect grasses and broadleaf weeds among cereal and broadleaf crops. The proximity based hyperspectral camera yielded hyperspectral resolution with high spatial resolution, enabling considerable spectral and spatial separation between crop and weed. In a different approach, Eddy et al. (2013) have investigated the feasibility of using reduced hyperspectral bandsets and ANN classification for discriminating between crop-field pea (*Pisum sativum*), spring wheat (*Triticum aestivum*), canola (*Brassica napus*) and weed-wild oat (*Avena fatua*), redroot pigweed (*Amaranthus retroflexus*). Reduced sets of narrow wave bands were created using Principal Component Analysis and Stepwise Discriminant Analysis with experimental results showing that plant discrimination using an ANN classifier was feasible and could provide considerable computational savings due to the reduced data dimensionality. The drawback however, was the high overhead required to train the classifier for successful operation.

This paper reports on recent results obtained from research into the development of an advanced proof-of-concept real-time plant discrimination system based on discrete spectral reflectance measurements for green-from-green plant discrimination. The developed system is tested for the discrimination of Anthurium (*Anthurium andraeanum*) from Sunkisses (*Ipomoea batatas* var. sunkisses) and Dandelion (*Taraxacum officinale*).

Experimental results show that practical green-from-green discrimination at a farming vehicle speed of 3 km/h can be achieved. At higher speeds, due to identified hardware limitations, the discrimination capability and accuracy declines.

2. System overview

The real-time Plant Discrimination Unit (PDU) is comprised of two 3-wavelength laser modules, two coated optical cavities, a high-speed linear photodetector array in the form of a line scan camera and an electronic circuit board housing six sub-modules, Fig. 1. These are a laser driver, analogue and digital power supply units, a temperature controller, a central processing unit, a spray nozzle activator and a line scan camera driver. The PDU is robustly packaged, using a rigid base plate and an accompanying light weight dust cover, to overcome harsh operation conditions such as shocks, vibrations and high temperatures.

The optoelectronic architecture of the PDU, as presented, has the following benefits:

1. The collimated, split laser beams enable spectral reflectance measurements to be taken from a small area of leaf of the target plant.
2. The laser module beam combiner/optical cavity design enables the laser beams to illuminate the same spot on the leaf, for all wavelengths, making the measured spectral reflectance spatially accurate with regards to different leaf morphologies.
3. The high dynamic range of the line scan sensor, when compared with area scan sensors of the type used in multi-spectral imaging, gives a better precision and a higher accuracy of the measured spectral properties.
4. The low complexity of the discrimination algorithm means that it is not computationally intensive, therefore providing true real-time performance.

2.1. Vegetation illumination

Fig. 2 shows the layout of the plant discrimination unit and illustrates how laser beams are generated to illuminate the vegetation.

2.1.1. Beam generation

Each laser module uses three 4 mm collimated laser sources, two red (635 nm and 685 nm) lasers and one near-infrared (785 nm), with output power levels of 30 mW, 50 mW and 50 mW, respectively. Within a module, each laser is independently mounted onto an alignment stage using alignment screws, so that all laser beams are aligned along the same optical axis. Two fixed,

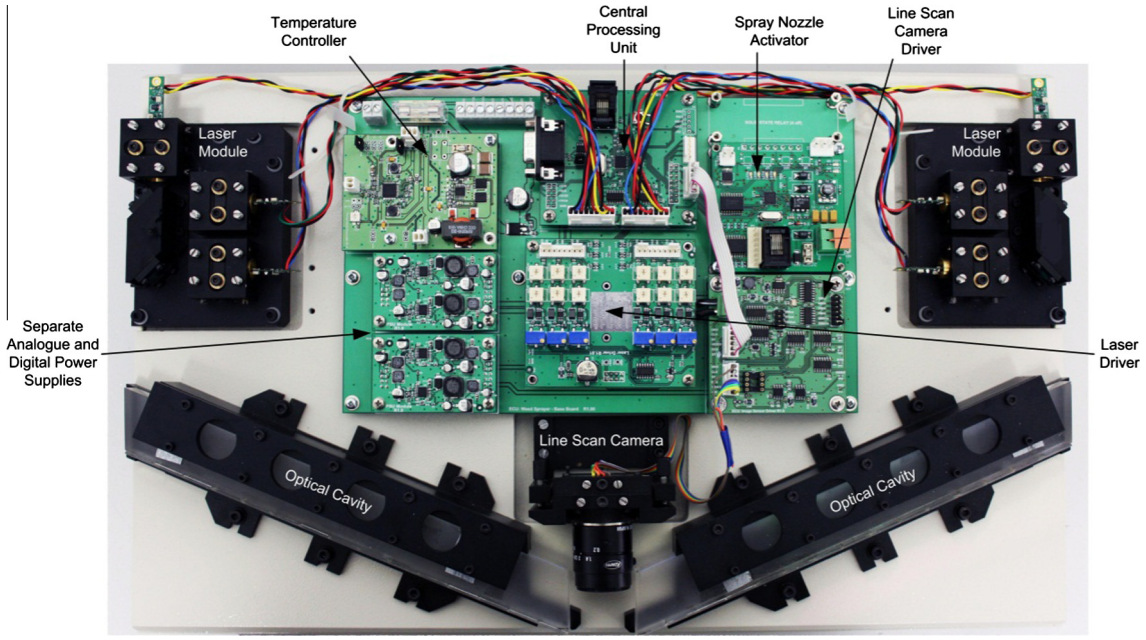

Fig. 1. Photograph of the developed real-time plant discrimination unit (PDU). It comprises two 3-laser modules with alignment and locking mechanisms, two optical cavities, a high-speed linear photodetector array in the form of a line scan camera and an electronic motherboard housing six daughter-boards, namely a laser driver, analogue and digital power supply units, a temperature controller, a central processing unit, a spray nozzle activator and a line scan camera driver.

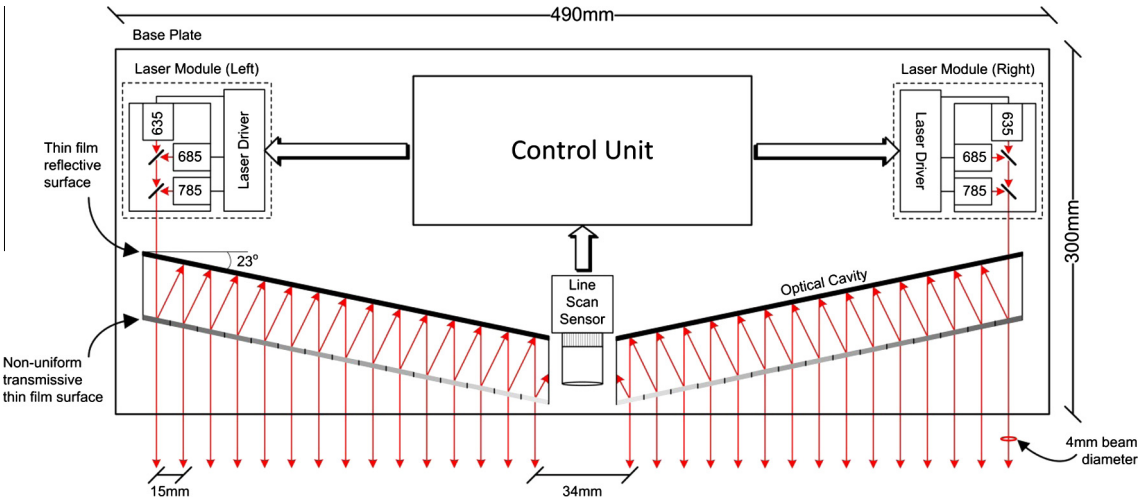

Fig. 2. Layout of the real-time plant discrimination unit, illustrating (laser) optical path and 4 mm collimated multi-spot beam generation over an approximate span of 450 mm.

thin-film beam combiners are used to combine the laser beams, as reported by Askraba et al. (2013). Once all laser beams emerging from the laser module are collinear, overlapped and their polarisation directions are aligned, all laser stages are secured with locking screws to prevent the lasers from moving during dynamic tests.

The collimated beams emerging from the laser module enter a multi-spot beam generator, which consists of an optical cavity coated with a reflective top (back) surface and non-uniform transmissive bottom (front) surface (Askraba et al., 2011, 2013). The beam spot field of view coverage was improved, in comparison to previously reported beam spot generators (Paap, 2014) by using a longer cavity inclined at a greater angle of 23°. This configuration increased the linear beam spacing from 12 mm in earlier prototypes to 15 mm in the final prototype and also reduced the gap between the two beams that are the closest to both sides of the line scan sensor. The non-uniform transmissive front surface was a fundamental improvement that enhanced overall system performance, leading to 4 mm wide collimated beams of almost similar intensities.

2.1.2. Line scan sensor

The stability of the measured reflected laser intensities was crucial to ensuring low false alarm rates as well as reliable and repeatable system performance. Accordingly, responsivity and switching speed were critical parameters in the choice of line scan sensor. A Hamamatsu S9227-03 CMOS linear image sensor, comprising a single line of 512 photodiodes, was used in the PDU shown in Fig. 1. In comparison to previously used sensors (Paap, 2014), the S9227-03 exhibited much lower variation in pixel response, Fig. 3, which yielded robust and repeatable measurements of spectral properties.

System tests revealed that the outdoor performance of the line scan sensor was noticeably degraded by ambient light, which, if bright enough, caused the sensor to saturate, negating any form of reliable spectral measurement. To address this problem and to remove much of the broadband solar noise, a dual band-pass optical filter (Fig. 4) with pass-bands specified at 648 ± 43 nm and 783 ± 29 nm for the red (635 nm, 685 nm) and NIR (785 nm) wavelengths respectively, was designed and fitted to the front of the sensor (Askraba et al., 2013; Paap, 2014).

Experimental outdoor tests with and without the solar filter, show an average reduction of ambient light in the order of 65–75%, as shown in Fig. 5.

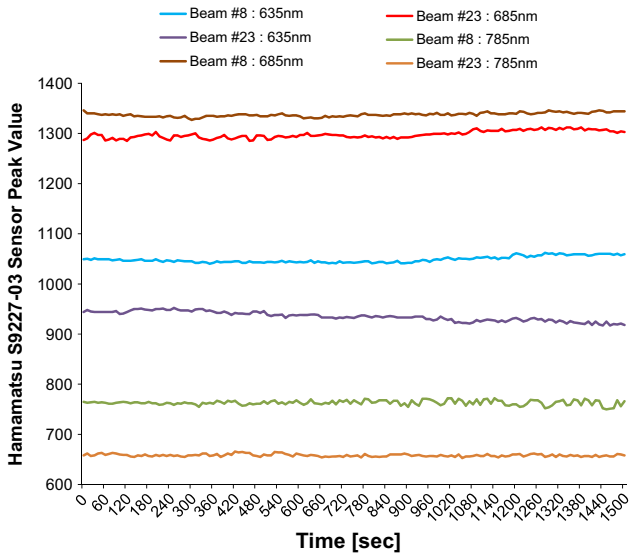

Fig. 3. S9227-03 sensor measured peak reflectance stability over a 25 min timeframe, for beam numbers 8 and 23. The PDU, mounted on a static holding frame, captured reflectance levels from a uniform green test card placed 950 mm vertically beneath the PDU, with the card sequentially illuminated by the individual 635 nm, 685 nm and 785 nm lasers.

From a system perspective, the solar filter effectively increased the sensor dynamic range, which in turn improved the optical signal-to-noise ratio (OSNR) of the measured spectral reflectance signal levels. For captured unfiltered/filtered measurements, the difference in the noise bandwidths of the data prevents direct comparison of signal-to-noise ratio improvements. A relative measure of the improvement in dynamic range is possible by defining the figure-of-merit (ρ):

$$\rho[i] = \frac{S[i]}{S[i] + N_{Ambient}[i]} \quad \text{for } i = 1..512$$

where $S[i]$ is the raw 10-bit signal value at pixel i and $N_{Ambient}[i]$ is the raw 10-bit background noise value at pixel i. Defining $\rho_{Unfiltered}$ and $\rho_{Filtered}$ as the figures-of-merit for unfiltered and filtered spectral reflectance measurements respectively, a measure of the relative improvement in the dynamic range is given by:

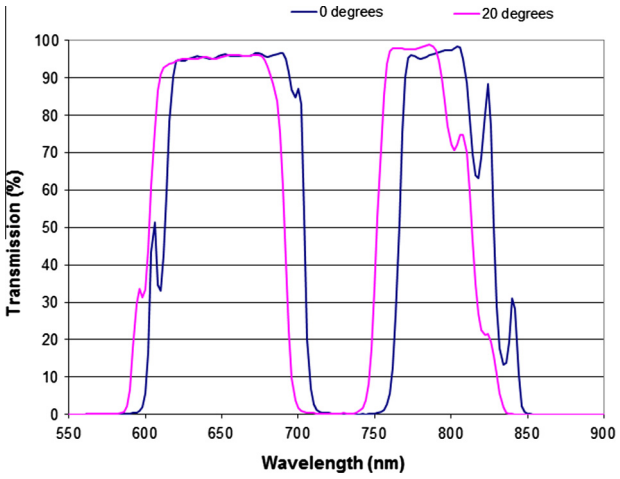

Fig. 4. Measured optical transmittance of the dual band-pass solar filter designed to reduce sensor noise due to ambient light level. Transmission characteristics of T_{635} = 95.7%, T_{685} = 96.1% and T_{785} = 95.8% were achieved for an incident angle of 0°, and T_{635} = 95.1%, T_{685} = 85.8% and T_{785} = 98.7% for an incident angle of 20°.

$$\Delta_{DR} = \frac{\rho_{Filtered}}{\rho_{Unfiltered}}$$

Experimental results illustrating the relative dynamic range improvement obtained on using the solar filter are presented in Figs. 6–8. The data was captured on an overcast day with a measured ambient light level of 4000 lux and an S9227-03 exposure time of 0.25 ms. The PDU, mounted on a static holding frame, captured reflectance levels from a uniform green test card placed 950 mm vertically beneath the PDU, with the card sequentially illuminated by the individual 635 nm, 685 nm and 785 nm lasers.

It is important to point out that the relative improvement of dynamic range is dependent upon the measurement conditions – laboratory, with artificial lighting; outdoors full shade, part shade, overcast or full sun with clear skies. Real-world statistical characterisation of the improvement in dynamic range is therefore complex.

2.2. Control unit

The control unit of the PDU encompasses the modules and functionality that allow for intelligent control of the optics unit, targeted spraying and external communications with the PDU.

2.2.1. Microcontroller

To perform successful discrimination and targeted spraying in real-time at adequate farming vehicle speeds, all requisite data acquisition and calculations must be completed within a fixed time frame. Failure to do so would mean that the system could inadvertently spray crops and not detected weeds.

For a collimated beam diameter of 4 mm, the processing time was constrained by the fact that on performing a measurement, the microcontroller must complete all calculations before the platform moves forward by 4 mm to the next measurement position. Fig. 9 shows the constrained processing time versus vehicle speed, for a 4 mm collimated beam diameter. It is clear from Fig. 9 that, for an initial target vehicle speed of 10 km/h, a processing time of 1.440 ms per discrimination cycle is required.

The microcontroller chosen to meet the processing time requirement was the Microchip dsPIC33F, which is a 16-bit, 40 MIPS digital signal controller with a modified Harvard architecture and direct support for both integer and Q15/Q30 fractional arithmetic. Theoretically, the microcontroller was capable of executing 57,600 instructions in 1.440 ms, which proved adequate for the

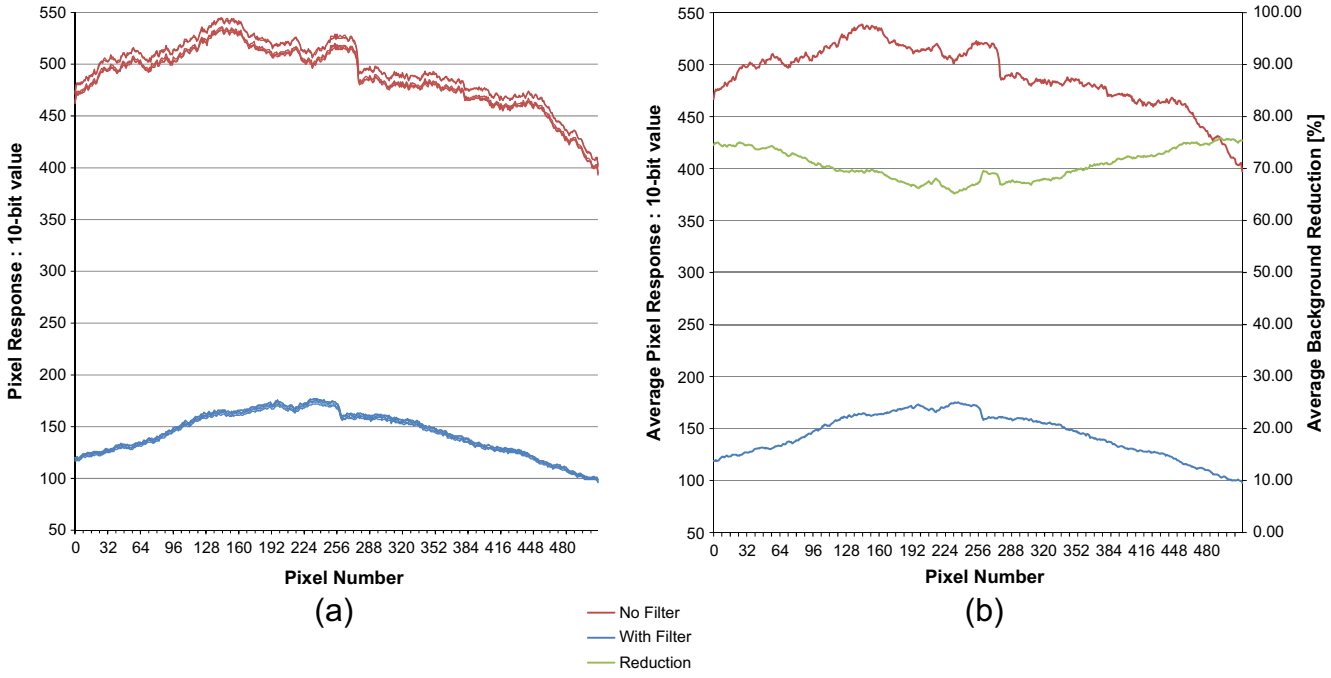

Fig. 5. PDU S9227-03 sensor response for (a) five sets of data captured with no solar filter and five sets of data captured with the designed solar filter. The average sensor response (b) shows a reduction of ambient light in the order of 65–75%. Data was captured on an overcast day, with a measured ambient light level of 4000 lux and an S9227-03 sensor exposure time of 0.25 ms. The PDU, mounted on a static holding frame, captured the ambient reflectance levels from a uniform green test card placed 950 mm vertically beneath the PDU.

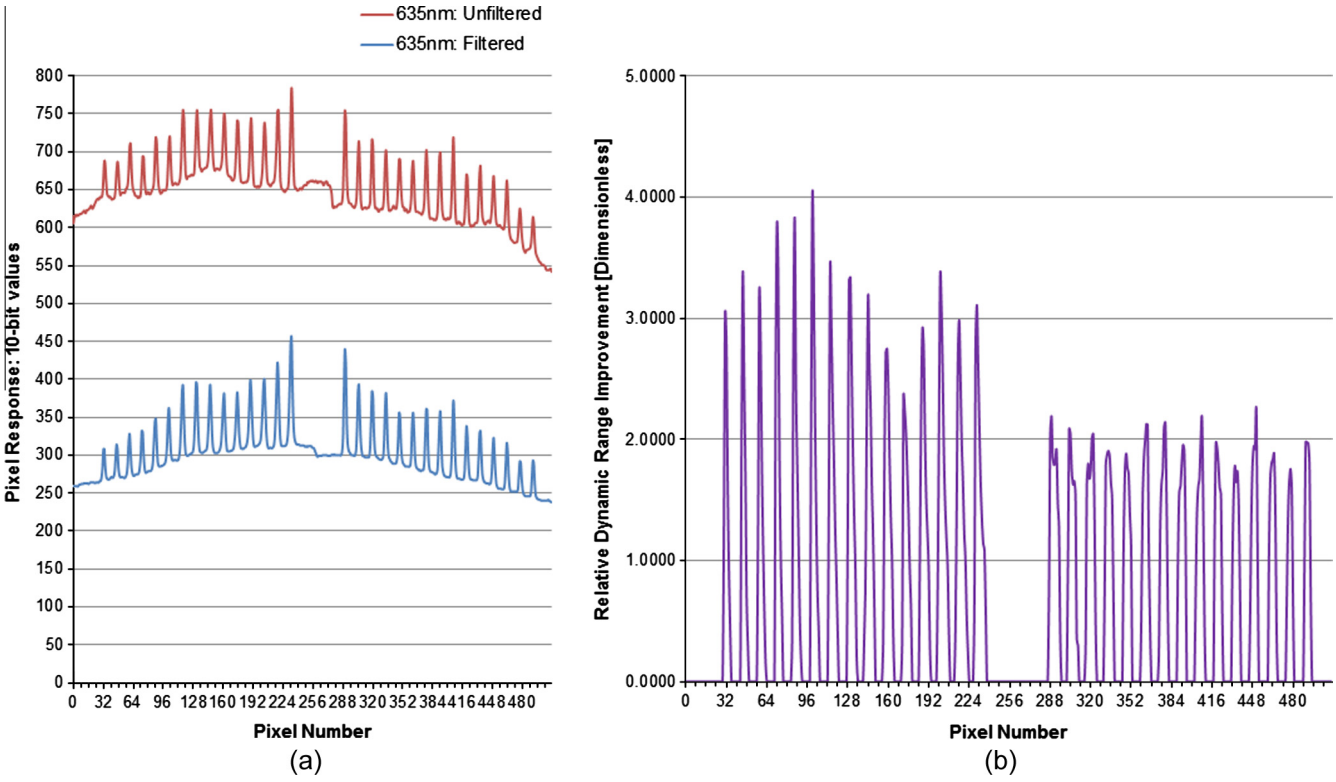

Fig. 6. (a) 635 nm wavelength raw 10-bit unfiltered/filtered spectral reflectance measurements. It is clear from the presented data that the solar filter effectively reduces the level of measured background noise due to the ambient light. (b) The relative improvement to the peak signal dynamic range, which can be attributed to the use of the dual band-pass solar filter.

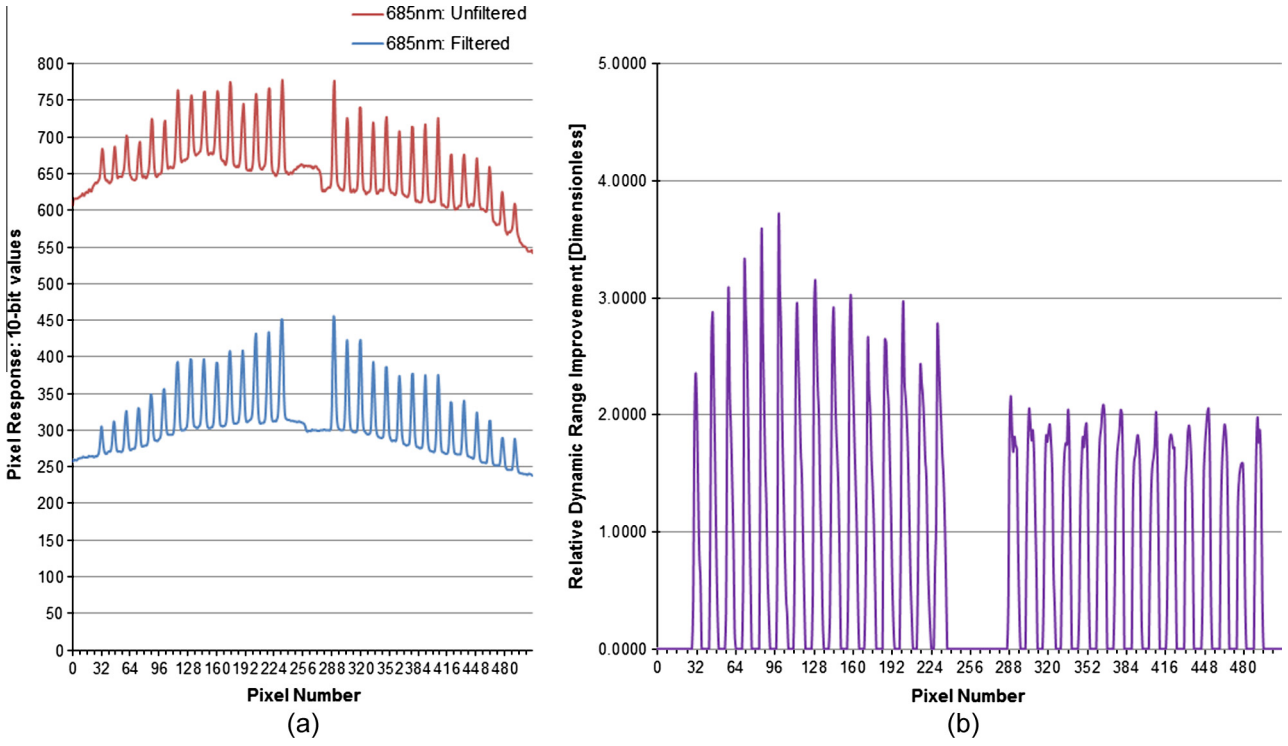

Fig. 7. (a) 685 nm wavelength raw 10-bit unfiltered/filtered spectral reflectance measurements. It is clear from the presented data that the solar filter effectively reduces the level of measured background noise due to the ambient light. (b) The relative improvement to the peak signal dynamic range which can be attributed to the use of the dual band-pass filter.

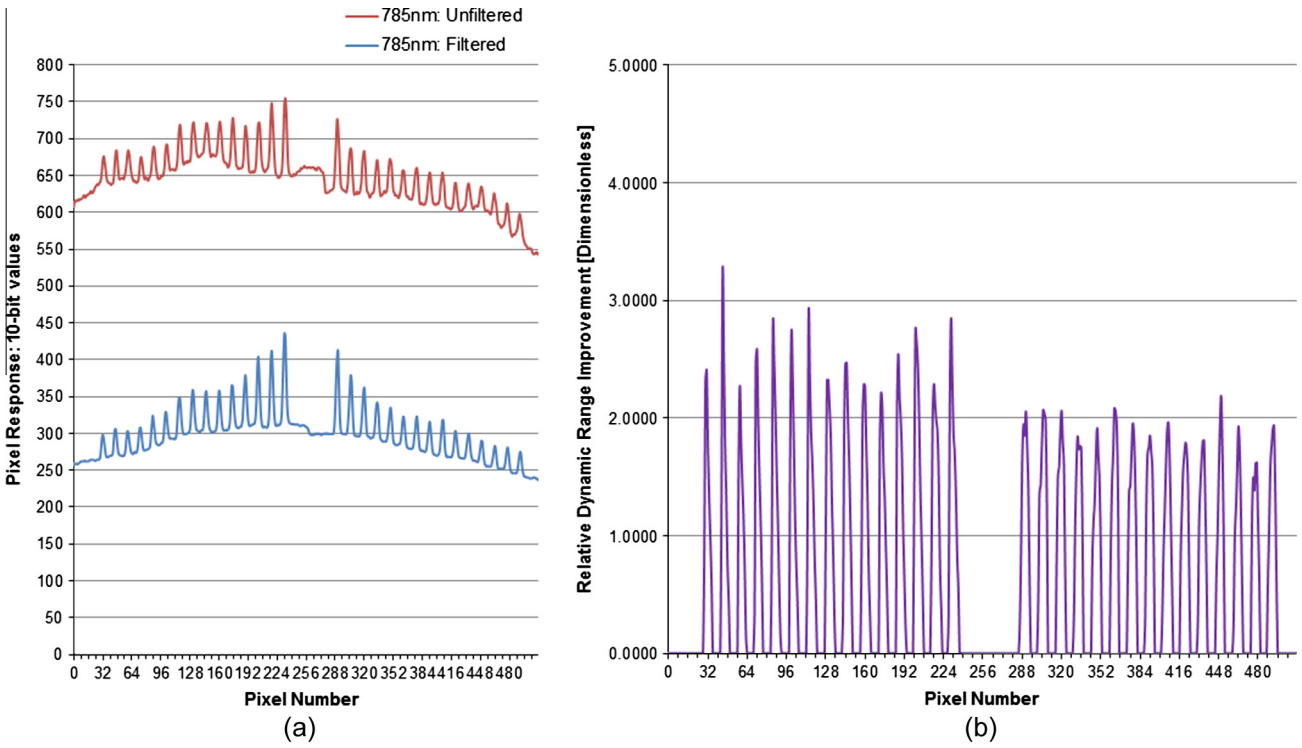

Fig. 8. (a) 785 nm wavelength raw 10-bit unfiltered/filtered spectral reflectance measurements. It is clear from the presented data that the solar filter effectively reduces the level of measured background noise due to the ambient light. (b) The relative improvement to the peak signal dynamic range which can be attributed to the use of the dual band-pass filter.

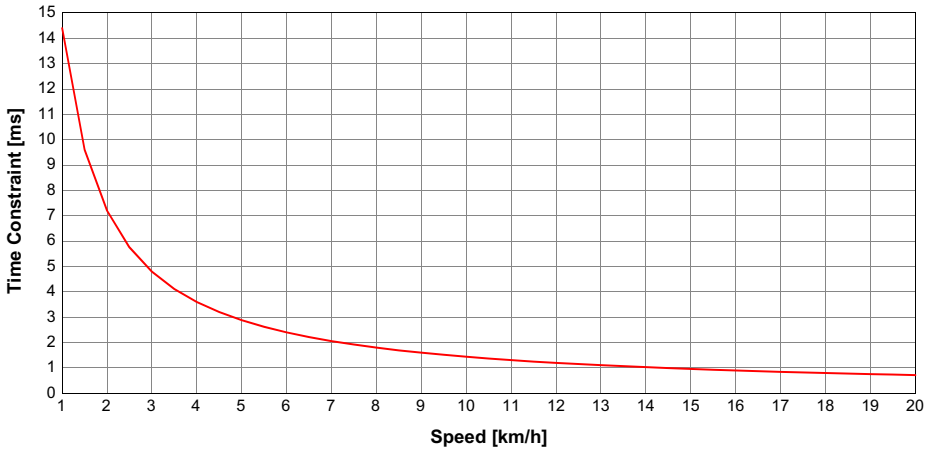

Fig. 9. Required processing time per discrimination cycle as a function of vehicle speed. For practical purposes, the operational speed is taken to be in the range of 10 km/h to 20 km/h, with 10 km/h being the initial targeted design speed.

low overhead discrimination algorithm, written in the C programming language.

The line scan data was acquired through a single channel of the multiplexed 13-channel on-chip analogue-to-digital converter, configured for 10-bit, 500 ksps operation. At 500 ksps operation, a single sensor read of 512-pixels took a time of 1.024 ms and this was a hardware-related limitation for operating the PDU at higher speeds. This is because four sensor reads are performed on a per scan basis amounting to a total sensor access time of 4.096 ms, which, after factoring in the processing time required by the discrimination algorithm, effectively limits the current vehicle speed at which the prototype PDU can operate, to around 3.5 km/h (Fig. 9).

3. Algorithm development and testing

Reliable and repeatable classification performance for real-time plant discrimination, using discrete spectral reflectance measurements, requires the identification of a set of spectral reflectance features for the target crops/weeds.

3.1. Spectral reflectance and defined discrimination parameters

The line scan sensor captures the diffuse, reflected light intensity from illuminated targets at the wavelengths (λ) 635 nm, 685 nm and 735 nm. The inferred target reflectance (Holland et al., 2012) for the individual beam-spots *i*, denoted as $R_{\lambda[i]}$, is calculated using the expression:

$$R_{\lambda[i]} = V_{\lambda[i]} N_{\lambda[i]} \quad \text{for } i = 1..512$$

where $V_{\lambda[i]}$ is the measured sensor response, in digital numbers of the ith beam and $N_{\lambda[i]}$, a normalisation factor for each beam, calculated as:

$$N_{\lambda[i]} = \frac{P_{ref}}{P_{\lambda[i]}}$$

The value P_{ref} is a reference beam optical power (BOP) and $P_{\lambda[i]}$, the optical power of the ith beam at wavelength λ.

With reference to a typical reflectance spectrum for a healthy plant leaf shown in Fig. 10, it is possible to define a set of features that, collectively, can be used for plant discrimination.

Various identified features are defined as follows:

1. Slopes S_1 and S_2: These measurements provide for green-from-green discrimination (Sahba et al., 2006; Paap et al., 2008) and are defined as:

$$S_1 \triangleq \frac{R_{635} - R_{685}}{\lambda_{685} - \lambda_{635}}$$

and

$$S_2 \triangleq \frac{R_{785} - R_{685}}{\lambda_{785} - \lambda_{685}}$$

2. Normalised Difference Vegetation (or Vegetative) Index (NDVI): The NDVI is a dimensionless quantity that provides a measure of whether the target under observation contains live vegetation or not. Healthy, living plants absorb most of the visible light that falls on them and reflect the NIR portion. In particular, the most defining information on vegetation is given by the difference in measured reflectance between the visible red and NIR wavelengths, as illustrated by the "red edge" of Fig. 10. Using these two bands, the NDVI is defined as:

$$\text{NDVI} \triangleq \frac{R_{\text{NIR}} - R_{\text{RED}}}{R_{\text{NIR}} + R_{\text{RED}}}$$

For the two red lasers of 635 nm and 685 nm wavelengths, it is possible to define the following NDVIs:

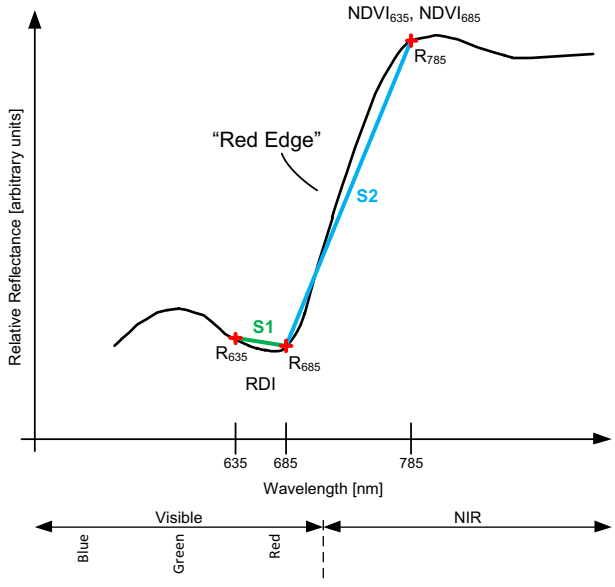

Fig. 10. Leaf reflectance as a function of wavelength, that is typical of a healthy plant. Those points that can be used to determine features for classification purposes have been highlighted for the applicable wavelengths.

$$\text{NDVI}_{635} \triangleq \frac{R_{785} - R_{635}}{R_{785} + R_{635}}$$

and

$$\text{NDVI}_{685} \triangleq \frac{R_{785} - R_{685}}{R_{785} + R_{685}}$$

On an individual basis NDVI_{685} can be used for green-from-brown discrimination (Paap, 2014).

3. Red Difference Index (RDI): This index is similar to the NDVI but is defined for the two red wavelengths as follows:

$$\text{RDI} \triangleq \frac{R_{635} - R_{685}}{R_{635} + R_{685}}$$

Note that not all of the identified parameters are necessarily suitable for green-from-green discrimination. The slope values S_1 and S_2 provided reliable green-from-green discrimination under static conditions in a controlled laboratory environment. However, in a dynamic outdoor environment it was found that platform dynamics and factors affecting reflection, such as the distance of the sensor from the leaf, the orientation of the leaf and the exposure time of the line scan sensor, collectively resulted in varying reflected laser intensities, which thwarted the usefulness of these two parameters. Data normalisation was able to remove many of the aforementioned factors and the NDVI_{635} and NDVI_{685} parameters were more reliable discriminants than the RDI parameter. It was experimentally found that, when an incident beam was illuminating a leaf, the variability in the red laser peak values led to errors in the measured spectral properties. With low red peak values, the variance of the RDI parameter was significantly larger than those of the NDVI parameters. This discovery discounted the use of the RDI parameter as a discriminant.

3.2. Discrimination algorithm

Fig. 11 shows a functional block diagram that details the data processing stages of the discrimination algorithm on a per scan basis, where, as illustrated, a single scan consists of:

1. Ambient light level measurement, with all lasers turned off.
2. 635 nm red laser reflectance measurement.
3. 685 nm red laser reflectance measurement.
4. 785 nm NIR laser reflectance measurement.

On a per scan basis, the individual measured reflectance levels were then adjusted by subtracting the measured background to produce three independent 512 element data vectors denoted by $\vec{V}_{635}$, $\vec{V}_{685}$ and $\vec{V}_{785}$. Using a defined peak threshold, T_{peak}, peak detection on the adjusted $\vec{V}_{785}$ values was performed. The peak detection algorithm scanned the $\vec{V}_{785}$ data for values above T_{peak}, performing two operations, namely, (1) single peak identification, representative of either a full leaf strike or ground strike, and (2) dual peak identification, representative of a partial leaf strike. For detected peaks corresponding to full leaf or ground strikes, the start pixel index, end pixel index and local maximum value were stored. Detected dual peaks corresponding to partial leaf strikes were flagged, as the peak information could not be used further by the discrimination algorithm. On completion, the output of the peak detection algorithm was a 1×30 vector denoted by $\vec{V}_{785\,PKs}$. Using the valid located peaks stored in $\vec{V}_{785\,PKs}$ the corresponding peak values in the $\vec{V}_{635}$, $\vec{V}_{685}$ and $\vec{V}_{785}$ vectors were extracted and the inferred target reflectance values calculated using measured BOP values stored in a lookup table (LUT).

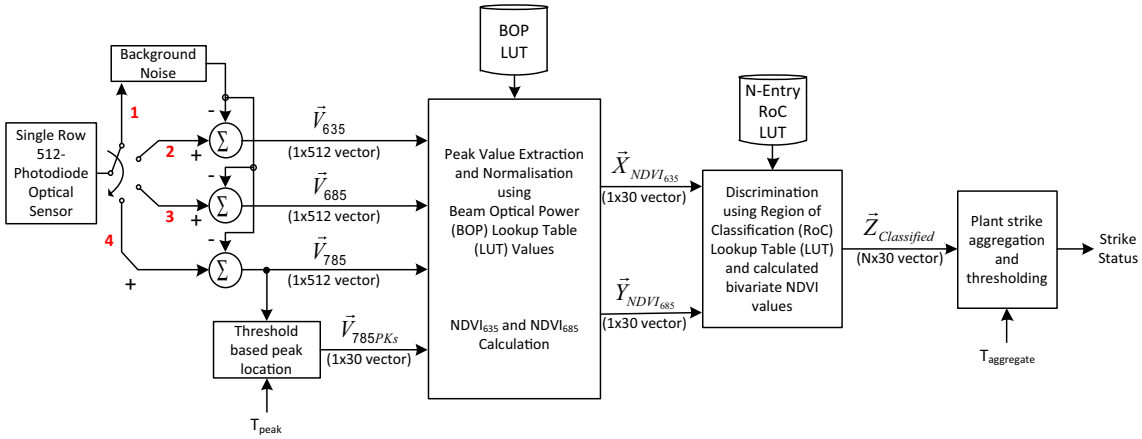

Fig. 11. Functional block diagram detailing the data processing stages of the discrimination algorithm implemented on the dsPIC33F embedded digital signal controller, on a per scan basis.

Finally, using the measured reflectance values, the corresponding 30 element $NDVI_{635}$ and $NDVI_{685}$ vectors, denoted by $\vec{X}_{NDVI_{635}}$ and $\vec{Y}_{NDVI_{685}}$, were calculated.

A green-from-brown test eliminated non-plant NDVI measurements, with subsequent plant discrimination achieved by classifying the calculated bivariate NDVI values for detected green plant material according to a predetermined Region-of-Classification (RoC) LUT. Depending upon the number of plant species N to be discriminated, the RoC LUT contained N parallelogram co-ordinate values that defined unique non-overlapping regions in $NDVI_{635}$ and $NDVI_{685}$ space. The discriminator output was an $N \times 30$ vector denoted by $\vec{Z}_{Classified}$, that contained all of the $NDVI_{635}$ and $NDVI_{685}$ data pairs allocated to one of the N possible predetermined regions-of-classification, where the vector length was determined by the maximum possible number of measurements on a per scan basis. $\vec{Z}_{Classified}$ was then processed for plant strikes, where a strike was deemed to have happened when measured NDVI values from an unwanted plant fell within a specified RoC. To reduce the false alarm rate of the algorithm and to improve the PDU's robustness and reliability, the strike detection algorithm was based on a running strike aggregate counter, which averaged the NDVI measurements of all of the individual beam strikes for a particular RoC. If a specified detection threshold $T_{aggregate}$ was exceeded, the strike was deemed valid and a plant spray signal generated.

Fig. 12. Illustration of the static experimental setup used for plant spectral reflectance measurements.

3.3. Test methodology

The performance of the developed PDU was evaluated under static and dynamic conditions with three broad leafed, potted plant species Anthurium (*Anthurium andraeanum*), Sunkisses (*Ipomoea batatas* var. sunkisses) and Dandelion (*Taraxacum officinale*).

For static tests, a vertically adjustable frame, shown in Fig. 12, was built to hold the PDU under test. Control data for determining the three regions-of-classification were captured under laboratory conditions using the 15 beams from one side of the PDU (Fig. 2). Experimentally, to reduce the measured reflectance of the scattered NIR wavelength, each sample leaf was placed on a 4 mm thick clear acrylic stage located on the floor. By adjusting the height of the PDU, the sample leaves were positioned at a distance of 900 mm above the sensor. To ensure that the reflectance measurements made were dominated by diffuse reflection and not biased by specular reflection captured by the line scan sensor, each leaf was tilted 25° with respect to the incident light. A single measurement trial, consisting of NDVI measurements for each of the individual 15 beams, was recorded for three different locations on the sample leaves, with care taken to avoid leaf midrib measurements. This generated a total of 45 static ($NDVI_{635}$, $NDVI_{685}$) measurement sets per sample leaf.

Dynamic outdoor tests were conducted with the PDU mounted on a frame attached to a motorised quad bike (Fig. 13). An aluminium shroud with plastic brushing down to the ground on the sides was used to block the ambient light level. The three test plants were placed in the ground along a defined test circuit and the quad bike driven around the circuit at an average speed of 3 km/h. On each pass of a detected test plant, the measured NDVI values were recorded.

Regions-of-classification defined using control data measured under laboratory conditions, offered a worst case test scenario

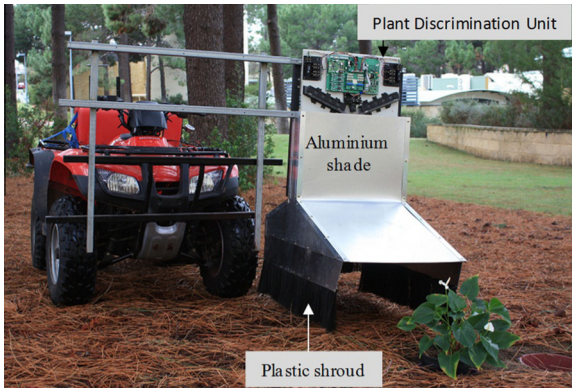

Fig. 13. Dynamic experimental setup used for plant spectral reflectance measurements. The PDU used is that shown in Fig. 1 and the visible plant is an Anthurium.

for evaluating the dynamic performance of the experimental proof-of-concept system. The capability of the system to discriminate the test plants outdoors, under different ambient lighting using NDVI values, calculated in real-time from dynamic spectral reflectance measurements, directly tests the practical validity of the dual NDVI discrimination approach.

4. Results and discussion

4.1. Static plant characterisation

Plotting the calculated bivariate $NDVI_{635}$, $NDVI_{685}$ values in the form of a scatter plot, for the measured test plant control data, revealed distinct, non-overlapping clusters, where the data groups displayed a definite linear dependency. This observed dependency can be attributed to the common 785 nm peak value used in the calculation of both NDVI parameters, which results in a weak positive correlation between the two values.

With reference to Fig. 14, which shows a scatter plot of ($NDVI_{635}$, $NDVI_{685}$) values for a single cluster of Anthurium, it is clear from the plotted data that it is possible to use a rectangle, rotated rectangle or parallelogram to define a unique RoC. A parallelogram based RoC provided an optimal enclosure to the data spread, with the lower and upper limits of the parallelogram specified by min{$NDVI_{685}$} and max{$NDVI_{685}$}, respectively.

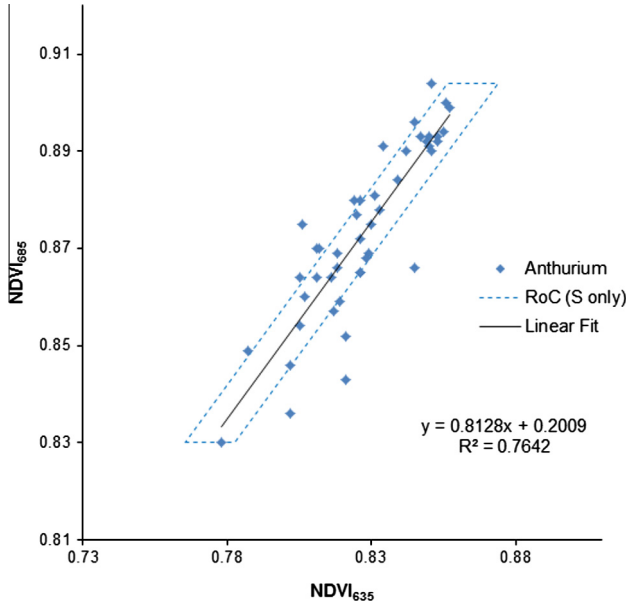

Fig. 14. Grouped Anthurium NDVI values calculated from the measured control data. Performing a linear fit to the points yields a reasonable coefficient of determination (R^2) and enables the determination of a parallelogram RoC using the calculated standard error (S) of the regression. For the illustrated RoC, 68% of observations should fall within ±S from the regression line, which is a quick approximation of the 68% prediction interval.

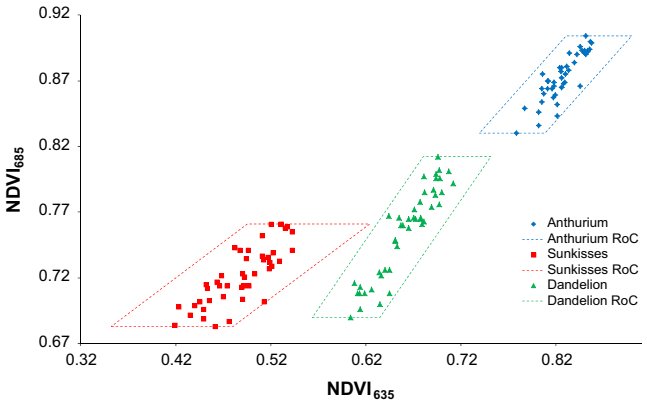

Fig. 15. NDVI scatter plot showing the regions-of-classification for the three test plants, under static laboratory conditions.

The angled sides of the parallelogram were determined through the application of regression analysis. A linear fit was performed on the data and the standard error (S) of the regression was calculated. In practical terms, the RoC determined from the measured control data, represents the range that a single new measurement is likely to fall within. Statistically, this range can be estimated using the standard error of the regression, to give a prediction interval. By linearly scaling S, it was possible to define an RoC so that it encompassed all of the control data for a test plant, without intersecting neighbouring regions-of-classification. Following this procedure, Fig. 15 shows the scatter plots for measured ($NDVI_{635}$, $NDVI_{685}$), for Anthurium, Sunkisses and Dandelion, under laboratory conditions. Three distinct regions-of-classification were clearly defined in Fig. 15 using scaling factors of 4, 5 and 3, which correspond to prediction intervals of 99.99%, 99.99% and 99.73% for Anthurium, Sunkisses and Dandelion, respectively.

In the experiments, the defined regions-of-classification were, at the lowest level, the decision rule for plant classification and subsequent strike event generation for dynamic system operation.

4.2. Dynamic performance

Two dynamic tests were performed. In the first, each plant was passed over 5 times at a speed of 3 km/h. Due to differences in plant sizes, a total of 916 NDVI measurements for Anthurium, 305 for Dandelion and 560 for Sunkisses were captured. The results obtained are presented in the form of scatter plots Figs. 16–18, with two scatter plots given per test plant. The first scatter plot displays the discrimination of the dynamic measurements for the test plant based on the defined regions-of-classification. The second scatter plot illustrates the spread of the measurements by plotting those that, whilst identified as green, fall outside the defined regions-of-classification. In the operational context of the proof-of-concept system, these results emphasise the effectiveness of adopting the regions-of-classification definition for accurate green-from-green plant discrimination.

It is clear from Figs. 16–18 that the control data captured under laboratory conditions resulted in sub-optimal regions-of-classification for testing the outdoor operation of the proof-of-concept system. Furthermore, the spread of the measurements for the individual test

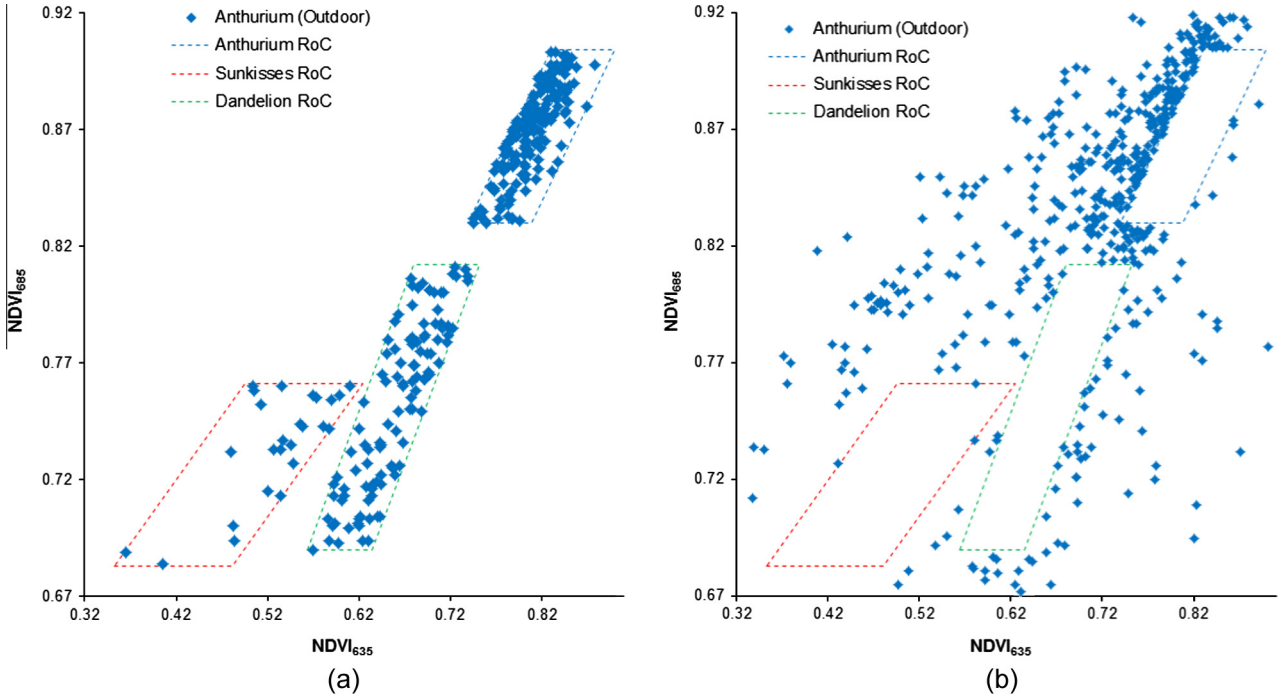

Fig. 16. (a) The discrimination of Anthurium at 3 km/h, using dual NDVI measurements calculated in real-time. Misclassification occurred with Anthurium NDVI values falling in the regions-of-classification for Sunkisses and Dandelion. However, through data aggregation the plant is identified as Anthurium. (b) Dual NDVI measurements that fall outside the defined regions-of-classification. These measurements illustrate the data spread arising from the complexities of performing dynamic measurements outdoors under real-world conditions.

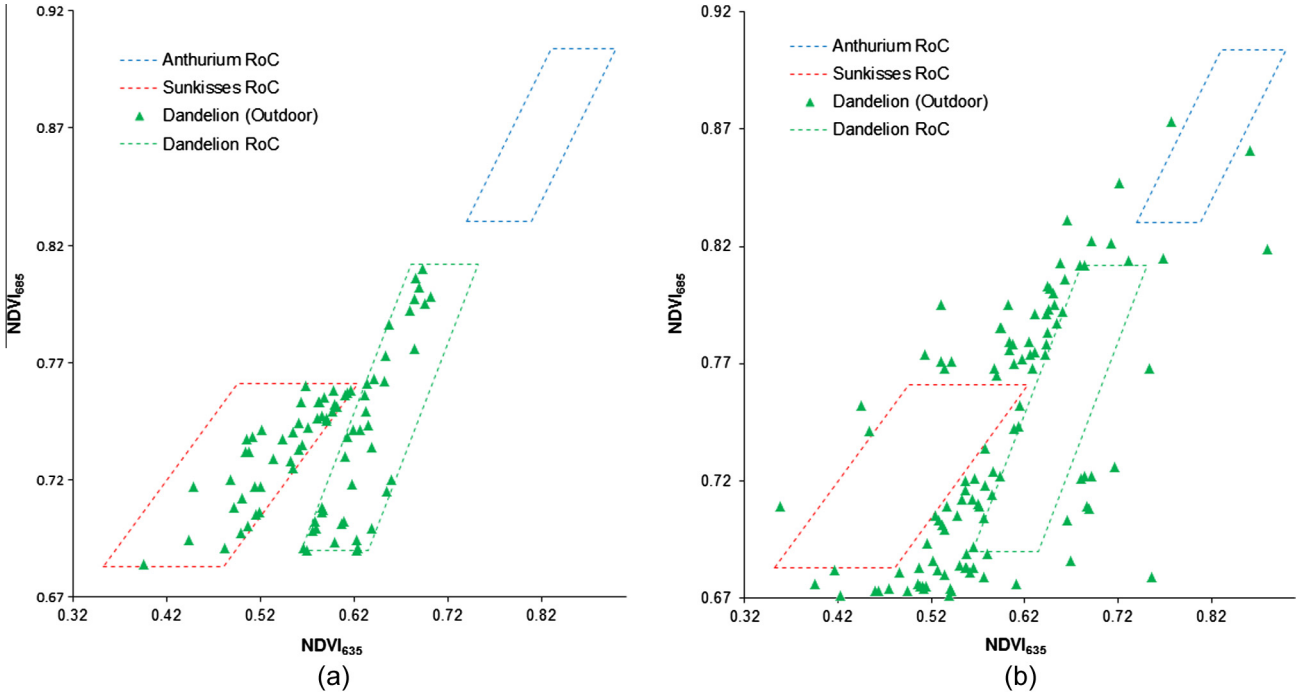

Fig. 17. (a) The discrimination of Dandelion at 3 km/h, using dual NDVI measurements calculated in real-time. Misclassification occurred with Dandelion NDVI values falling in the RoC for Sunkisses, however, through data aggregation the plant cannot be identified as Dandelion. (b) Dual NDVI measurements that fall outside the defined regions-of-classification.

plants illustrates the complexity arising from data variability obtained on performing dynamic measurements outdoors, under real-world conditions.

In the second test, two trials, consisting of 2 scans per plant per trial, were conducted at a vehicle speed of 3 km/h. In this test, dual NDVI measurements falling within the defined regions-of-classification

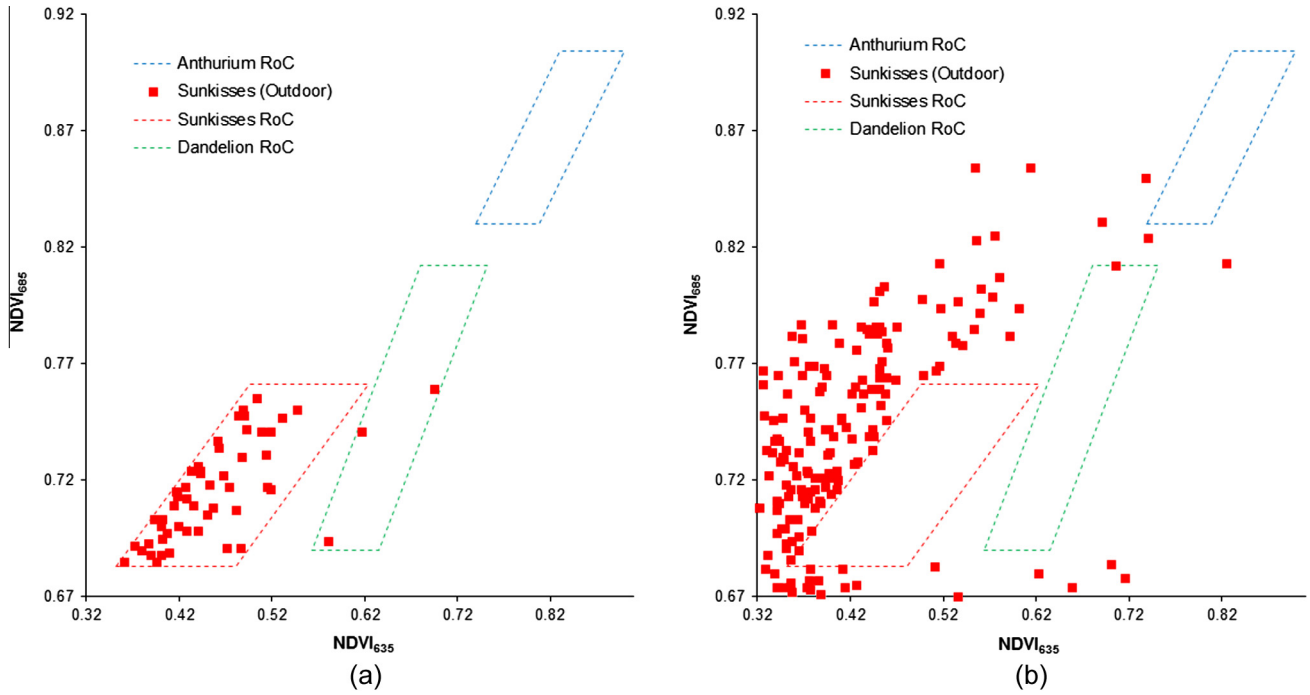

Fig. 18. (a) The discrimination of Sunkisses at 3 km/h, using dual NDVI measurements calculated in real-time. Misclassification occurred with Sunkisses NDVI values falling in the RoC for Dandelion, however, through data aggregation the plant is identified as Sunkisses, (b) dual NDVI measurements that fall outside the defined regions-of-classification.

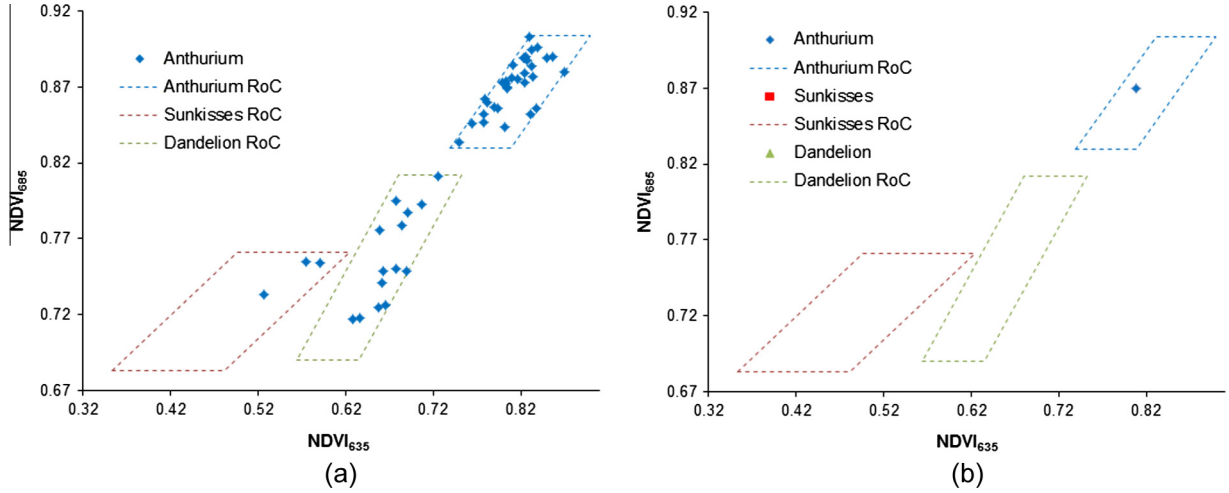

Fig. 19. (a) Distribution of the dual NDVI values calculated from the real-time spectral reflectance measurements for Anthurium, for a vehicle speed of 3 km/h. With no data aggregation the misclassification of Anthurium as Sunkisses and Dandelion, degrades system performance. (b) Correct discrimination algorithm output for a data aggregation threshold of 15. The single point is the calculated mean of the bivariate ($NDVI_{635}$, $NDVI_{685}$) data.

were aggregated, with an experimental aggregation threshold used to generate a single plant strike decision. The aggregation threshold was manually set so that the effects of threshold level on system performance could be ascertained. Measured dual NDVI values falling outside the regions-of-classification were ignored. In the first trial, Anthurium and Dandelion were the target plants, while in the second trial, the target plants were Sunkisses and Dandelion. For ease of interpretation, the results obtained are presented in the form of scatter plots in Figs. 19–22, with two scatter plots given per test plant. The first scatter plot displays the distribution of the accepted dual NDVI values calculated from the measured spectral reflectance, with respect to the defined regions-of-classification. The second scatter plot illustrates the discrimination algorithm output after aggregating and thresholding the accepted NDVI values.

Fig. 19(a) shows the distribution of the calculated dual NDVI values for Anthurium, for a vehicle speed of 3 km/h. It is noticed that with no NDVI aggregation, overlap of the regions-of-classification leads to the misclassification of Anthurium as

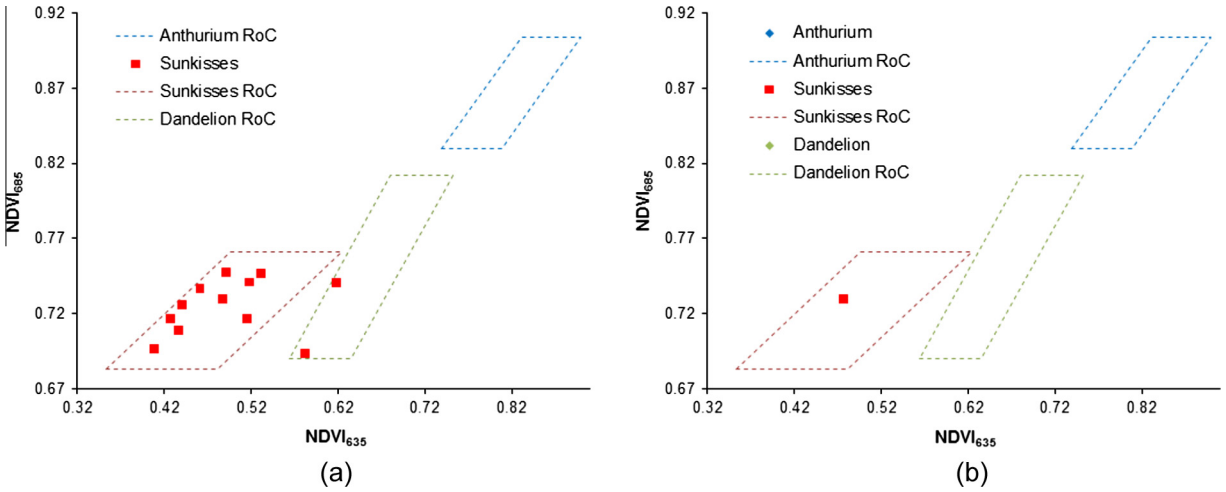

Fig. 20. (a) Distribution of the dual NDVI values calculated from the real-time spectral reflectance measurements for Sunkisses, for a vehicle speed of 3 km/h. With no data aggregation the misclassification of Sunkisses as Dandelion, degrades system performance. (b) Correct discrimination algorithm output for a data aggregation threshold of 3. The single point is the calculated mean of the bivariate ($NDVI_{635}$, $NDVI_{685}$) data.

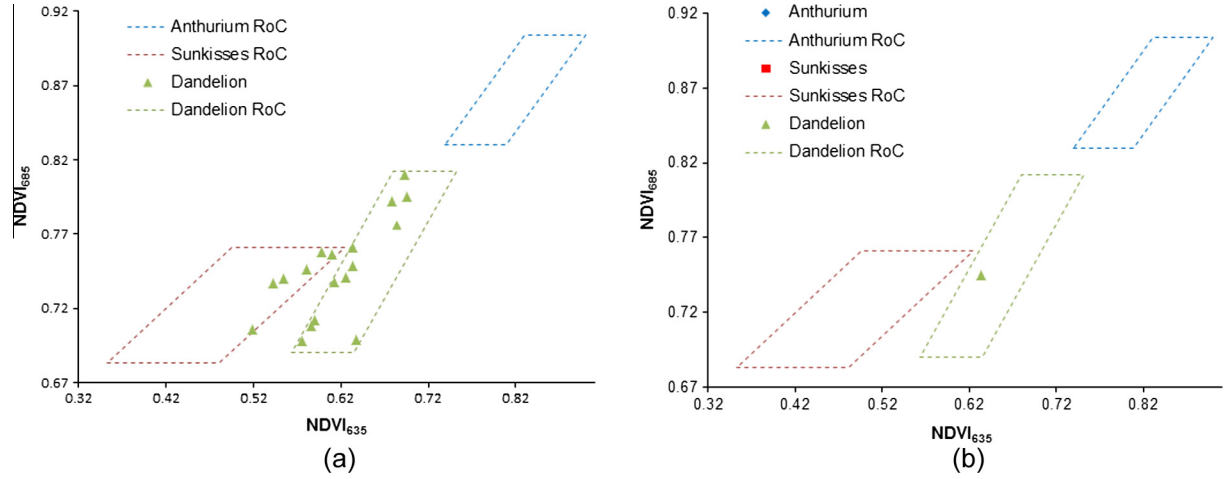

Fig. 21. (a) Distribution of the dual NDVI values calculated from the real-time spectral reflectance measurements for Dandelion, for a vehicle speed of 3 km/h. With no data aggregation the misclassification of Dandelion as Sunkisses, degrades system performance. (b) Correct discrimination algorithm output for a data aggregation threshold of 7. The single point is the calculated mean of the bivariate ($NDVI_{635}$, $NDVI_{685}$) data.

Sunkisses and Dandelion, thus degrading the accuracy of the PDU. Fig. 19(b) shows the distribution of the NDVI values for Anthurium when the discrimination algorithm included data aggregation with a threshold of 15. In this case, a single point, representing the mean of the bivariate ($NDVI_{635}$, $NDVI_{685}$) data, is displayed in the RoC of Anthurium, indicating a correct discrimination result.

Fig. 20(a) shows the distribution of the dual NDVI values calculated from the spectral reflectance measurements for Sunkisses, for a vehicle speed of 3 km/h. With no data aggregation, overlap is seen between the regions-of-classification for Sunkisses and Dandelion, leading to the misclassification of Sunkisses as Dandelion. Using data aggregation with a threshold of 3, a single point can be attained in the RoC of Sunkisses, as displayed in Fig. 20(b).

The distribution of the dual NDVI values for Dandelion is shown in Fig. 21(a), for a vehicle speed of 3 km/h. Again, the overlap between the regions-of-classification for Dandelion and Sunkisses is overcome using data aggregation with a threshold of 7, as evidenced from Fig. 21(b).

Finally, it is important to mention that when the vehicle speed was increased to 6 km/h, the aggregation algorithm failed to discriminate between Dandelion and Sunkisses even when thresholding has been optimised. In this case, the distribution of the dual NDVI values for Dandelion is shown in Fig. 22(a).

The overlap between the regions-of-classification for Dandelion and Sunkisses cannot be overcome using strike aggregation with an optimum threshold of 10, as evidenced from Fig. 22(b). This is attributed to the real-time processing constraint discussed in Section 2.2.1. The improvement of the discrimination accuracy at high vehicle speeds requires (i) a higher speed, low noise, high sensitivity line scan sensor, (ii) a faster analogue-to-digital converter, and (iii) reduction of the exposure time of the sensor, which depends on the output laser intensities.

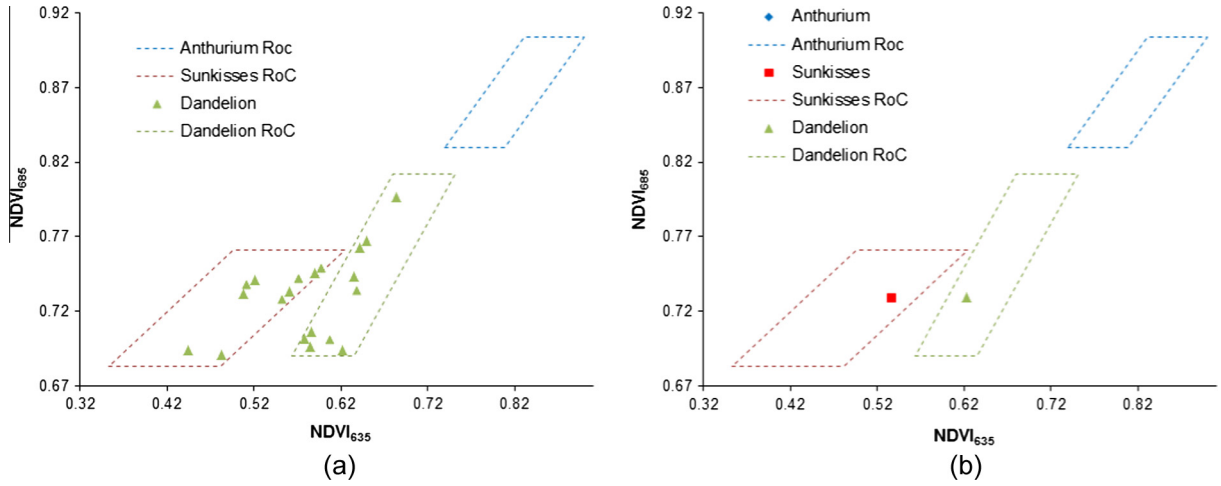

Fig. 22. (a) Distribution of the dual NDVI values calculated from the real-time spectral reflectance measurements for Dandelion, for a vehicle speed of 6 km/h. (b) Discrimination algorithm output for a data aggregation threshold of 10. The two individual points are the calculated mean of the relevant bivariate ($NDVI_{635}$, $NDVI_{685}$) data. In this particular sweep, the algorithm has determined an equal dual NDVI strike rate for both Sunkisses and Dandelion. This type of scenario cannot be handled by simply aggregating and thresholding the dual NDVI values.

5. Conclusion

The performance of an advanced real-time plant discrimination system, employing two red laser diodes (635 nm, 685 nm) and one near-infrared laser diode (785 nm) in conjunction with a linear sensor array, has been investigated experimentally. Experimental results have shown that the use of dual Normalised Difference Vegetation Indices (NDVI) in conjunction with data aggregation and threshold optimisation significantly enhances the green-from-green discrimination capability of the plant discrimination system.

The outdoor performance of the advanced real-time plant discrimination system has been evaluated, using three different plant species, Anthurium, Sunkisses and Dandelion. Experimental results have demonstrated that the system can attain reliable plant detection and practical discrimination at a vehicle speed of 3 km/h.

Future work is focusing on (a) achieving high detection accuracy at a target vehicle speed of 10 km/h, by addressing known system limitations, (b) further researching the concept of aggregating and thresholding plant NDVI measurements within defined regions-of-classification with the objective of statistically based automated threshold determination, for making single plant strike decisions, and (c) the statistical determination of optimal regions-of-classification for calibrating the PDU in-situ, prior to use.

Acknowledgements

This research is financially supported by the Australian Research Council and Photonic Detection Systems Pty. Ltd.

References

Askraba, S., Paap, A., Alameh, K., Rowe, J., 2011. Design of laser multi-beam generator for plant discrimination. In: High Capacity Optical Networks and Enabling Technologies (HONET), pp. 26–29.

Askraba, S., Paap, A., Alameh, K., Rowe, J., Miller, C., 2013. Optimization of an optoelectronics-based plant real-time discrimination sensor for precision agriculture. J. Lightwave Technol. 31 (5), 822–829.

Brownhill, D., 2006. Using 'Weedseeker' spot spraying technology in cropping systems. In: Proceedings of the 10th Annual Symposium on Precision Agriculture in Australasia, Sydney, Australia.

Deng, W., Huang, Y., Zhao, C., Wang, X., 2014. Discrimination of crop and weeds on visible and visible/near-infrared spectrums using support vector machine, artificial neural network and decision tree. Sens. Transducers 26 (special issue), 26–34.

Eddy, P.R., Smith, A.M., Hill, B.D., Peddle, D.R., Coburn, C.A., Blackshaw, R.E., 2013. Weed and crop discrimination using hyperspectral image data and reduced bandsets. Can. J. Remote Sens. 39 (6), 481–490.

Felton, W.L., McCloy, K.R., 1992. Spot spraying. Agric. Eng. 73 (6), 9–12.

Holland, K.H., Lamb, D.W., Schepers, J.S., 2012. Radiometry of proximal active optical sensors (AOS) for agricultural sensing. IEEE J. Sel. Top. Appl. Earth Obs. Remote Sens. 5 (6), 1793–1802.

Noble, S.D., Brown, R.B., Crowe, T.G., 2002. The use of spectral properties for weed detection and identification – a review. In: AIC 2002 Meeting, CSAE/SCGR Program, Saskatoon, Saskatchewan.

Paap, A., Askraba, S., Alameh, K., Rowe, J., 2008. Photonic-based spectral reflectance sensor for ground-based plant detection and weed discrimination. Opt. Express 16 (2), 1051–1055.

Paap, A., 2014. Development of an Optical Sensor for Real-time Weed Detection using Laser based Spectroscopy. PhD Thesis. Electron Science Research Institute, Edith Cowan University.

Sahba, K., Askraba, S., Alameh, K.E., 2006. Non-contact laser spectroscopy for plant discrimination in terrestrial crop spraying. Opt. Express 14 (25), 12485–12493.

Shapira, U., Herrmann, I., Karnieli, A., Bonfil, D.J., 2010. Weeds detection by ground-level hyperspectral imaging. In: Proceedings of Hyperspectral Workshop 2010, Frascati, Italy.

Wang, N., Zhang, N., Dowell, F.E., Sun, Y., Peterson, D.E., 2001. Design of an optical weed sensor using plant spectral characteristics. Trans. ASAE 44 (2), 409–419.

Zhang, N., Wang, M., Wang, N., 2002. Precision agriculture – a worldwide overview. Comput. Electron. Agric. 36, 113–132.

Zwiggelaar, R., 1998. A review of spectral properties of plants and their potential use for crop/weed discrimination in row-crops. Crop Prot. 17 (3), 189–206.